applied optics

# Partially coherent noise-like pulse generation in amplified spontaneous Raman emission

Qing Zhao,[1,2] Weiwei Pan,[2,3,4] Xianglong Zeng,[1] and Yan Feng[2,*]

[1]Key Laboratory of Specialty Fiber Optics and Optical Access Networks, School of Communication and Information Engineering, Shanghai University, Shanghai 200072, China
[2]Shanghai Institute of Optics and Fine Mechanics, Chinese Academy of Sciences, and Shanghai Key Laboratory of Solid State Laser and Application, Shanghai 201800, China
[3]University of the Chinese Academy of Sciences, Beijing 100049, China
[4]e-mail: bfoga38253@163.com
*Corresponding author: feng@siom.ac.cn

Received 20 November 2017; revised 25 January 2018; accepted 26 February 2018; posted 26 February 2018 (Doc. ID 313785); published 20 March 2018

**Amplified spontaneous Raman emission under picosecond pulse pumping is studied in detail both experimentally and numerically. It is found that the Raman output pulses are noise-like with partial coherence, which has important implications for various applications. Numerical simulation reproduces the finding well, along with the temporal and spectral dependence of the Raman pulse on the pump pulse energy. The numerical simulations of the temporal, spectral, and energy evolution of the Raman and pump pulse along the fiber gives insight on how to design such sources.** 

***OCIS codes:*** (140.3550) Lasers, Raman; (060.2310) Fiber optics; (190.5650) Raman effect.

https://doi.org/10.1364/AO.57.002282

## 1. INTRODUCTION

Ultrafast fiber lasers have been proven to have extensive applications in industry, medicine, defense, and scientific research [1–5]. Usually ultrafast fiber lasers use rare-earth-doped fibers as a gain medium, which, however, can emit ultrashort pulses only in limited spectral range. Stimulated Raman scattering (SRS) has the advantage of wavelength agility as a gain mechanism, which can solve the problem of limited gain bandwidth of the rare-earth-doped fibers, and extend the field of application of ultrafast pulsed lasers.

Compared with the Raman lasers based on a mode-locked oscillator, amplified spontaneous Raman emission (ASRE) by pulse pumping is a simpler method to generate a wavelength-agile ultrafast laser. Such sources open up new possibilities in spectroscopy and photoacoustic imaging, etc. [6,7]. Note there were a number of studies on the noise characteristics in ASRE [8,9]. But the characteristics of the ultrafast pulse generated by amplified spontaneous Raman scattering have never been investigated carefully, which are very important for the applications.

In this paper, we investigate the pulse characteristics of ASRE under picosecond pulse pumping both experimentally and numerically. Notably, it is found experimentally for the first time that the Raman output pulses are noise-like but with partial coherence, which has important implications for various applications. With a model based on the generalized nonlinear Schrödinger equation (GNLSE), numerical simulations reproduce the finding well, along with other experimental observations including Raman pulse energy and spectrum dependence on pump pulse energy. The numerical simulations also give us insight on the Raman and pump pulse evolution along the fiber, which cannot be observed experimentally without much effort.

## 2. EXPERIMENTAL SETUP AND RESULTS

An experimental diagram of the amplified spontaneous Raman emission generation is shown in Fig. 1. The pump pulse is based on a mode-locked fiber laser that can emit a near transform-limited soliton pulse with a pulse width of 15 ps and a spectral width of 0.1 nm. In order to increase the walk-off length between the pump pulse and Raman pulse, the pump pulse is broadened by going through a long piece of single-mode fiber before amplification. The pump pulse is broadened to about 45 ps and the spectral width is 3 nm. The Raman fiber is a piece of 60 m long PM980 fiber. After the Raman fiber, a 1064/1120 nm wavelength-division multiplexer (WDM) is used to separate Raman light and residual pump laser.

The ASRE reaches a critical point at a pump pulse energy of 15 nJ. The pulse energy of the Raman light is plotted against the pump pulse energy in Fig. 2(a). Near the point, the output experiences a gradual increase, which is a typical feature of

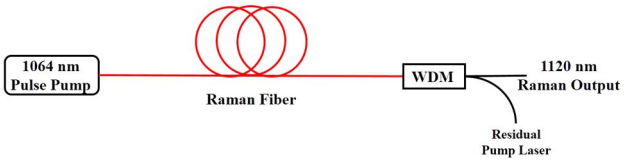


**Fig. 1.** Schematic diagram of the amplified spontaneous Raman emission generation. WDM, wavelength-division multiplexer.

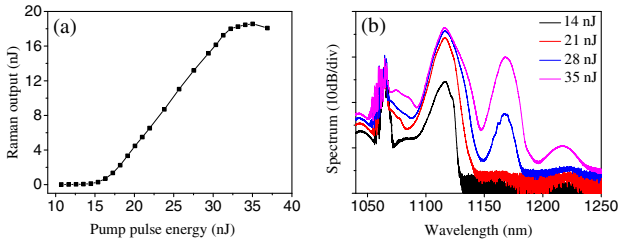


**Fig. 2.** (a) Pulse energy of the Raman light as a function of the pump pulse energy; (b) spectra of the Raman light at different pump pulse energies.

spontaneous Raman emission generation and amplification. After the point, the output increases linearly with respect to the pump power. A maximum of 19 nJ at 1120 nm is obtained at a pump pulse energy of 35 nJ. Further increase of the pump pulse energy results in a drop-off in output due to the generation of the second Raman Stokes light. Spectra of the Raman light under several pump pulse energies are presented in Fig. 2(b), which shows the evolution of Raman light with increasing pump pulse energy. At high pump pulse energy, the second Raman Stokes light increases quickly and the first Raman Stokes light stops increasing.

Because temporal details of the Raman output pulses with width in the level of picosecond cannot be resolved by common oscilloscopes, a commercial autocorrelator is used to investigate characteristics of the Raman pulses in the time domain. An autocorrelation trace of the Raman light at a pump pulse energy of 33 nJ is presented in Fig. 3(a) as a typical example. It shows a narrow spike on a wide pedestal. Such a pulse is considered as a noise-like pulse [10–14], which is in fact a packet of fluctuating and stochastic subpulses. It has lower coherence but higher peak power when compared to regular ultrashort pulses with

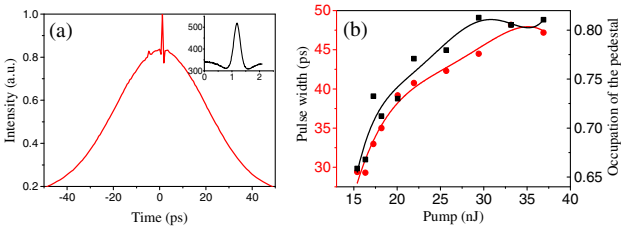


**Fig. 3.** (a) Autocorrelation trace of the Raman light under a pump pulse energy of 33 nJ. Inset: a zoom-in of the AC peak. (b) The width (circle) and normalized height (box) of the autocorrelation pedestal versus pump.

the same overall width. Therefore, noise-like pulses have extensive applications in harmonic generation [15], Raman conversion [16,17], and supercontinuum generation [18–23], as well as applications in imaging and sensing systems with high temporal and/or spatial resolution [24].

Pulse width defined as full wave at half-maximum of the pedestal is plotted against the pump pulse energy in Fig. 3(b). The pulse width increases together with the pump pulse energy, which is caused by the threshold effect and femtosecond energy transferring in SRS, and also other nonlinear effects.

Normalized height of the pedestal in the autocorrelation trace contains information on the correlation among the subpulses and the coherence of the pulses. For pulses consisting of complete random subpulses, the normalized height of the autocorrelation trace pedestal is 0.5; a normalized height of larger than 0.5 means existence of coherence in noise-like pulses [25]. The normalized height of the pedestal is plotted as a function of pump pulse energy in Fig. 3(b) as well. It is found that the normalized height is always larger than 0.5 and increases with respect to pump pulse energy, and the highest height is 0.81. This means that the noise-like pulses generated by amplified spontaneous Raman emission are partially coherent, which has never been noticed and discussed in the literature. Since ASRE is a simple method to obtain wavelength-flexible partially coherent picosecond noise-like pulses and has numerous applications, it is significative to make a detailed investigation about it.

## 3. NUMERICAL MODEL

In order to understand the pulse formation process in ASRE, a model based on the GNLSE is used to simulate pulse evolution in the Raman fiber:

$$\frac{\partial A}{\partial z}+\frac{\alpha}{2}A+\frac{i\beta_2}{2}\frac{\partial^2 A}{\partial T^2} = i\gamma\left(A(z,T)\int_{-\infty}^{\infty}R(T')|A(z,T-T')|^2\mathrm{d}T'\right). \quad (1)$$

The left-hand side of Eq. (1) models linear propagation effects, $A$ denotes the slowly varying pulse envelope of the pulse, $z$ refers to the pulse propagation distance, $T$ is the pulse local time, $\alpha$ indicates the linear power attenuation, and the $\beta_2$ is the group velocity dispersion [26], which causes pulse broadening. The right-hand side models nonlinear effects, concluding self-phase modulation (SPM), and Raman effects. $\gamma$ is the nonlinear coefficient. $R(t)$ is the nonlinear response function, including SPM and Raman response function $h_R(t)$, it is modeled as [27]

$$\begin{aligned} R(t) &= (1-f_R)\delta(t)+f_R h_R(t) \\ &= (1-f_R)\delta(t) \\ &\quad + f_R\frac{\tau_1^2+\tau_2^2}{\tau_1\tau_2^2}\exp(-t/\tau_2)\sin(t/\tau_1)\Theta(t), \end{aligned} \quad (2)$$

where $f_R = 0.18$ is the fractional contribution of the delayed Raman response [27–29], which is calculated by the peak Raman gain, $\tau_1$ is 12.2 fs, and $\tau_2$ is 32 fs [27]. $\Theta(t)$ is the Heaviside step function and $\delta(t)$ is the Dirac delta function [26]. The time domain of the $h_R(t)$ can be speculated by the Raman gain spectrum. More accurate forms of the

Raman response function have also been investigated by Hollenbeck and Cantrell [30].

The process of ASRE under picosecond pulse pump is simulated by solving the model with the fourth-order Runge–Kutta method, which has been proven valid in simulation of supercontinuum generation [26,31] and synchronously pumped Raman fiber laser [32]. Similar to the experiment, the pump pulse is also a transform-limited sech pulse with a temporal width of 15 ps first in the simulation. Then the transform-limited pulse goes through a long piece of fiber to be broadened in both the time and frequency domains. When the length of the long fiber is about 200 m, the temporal and spectral widths of the pump pulse are close to the experiment. The energy of the pump pulse is adjusted by changing the pulse peak power and the pulse duration keeps unchanged. A white Gaussian noise with an average power of $10^{-9}$ W is added in the base of the pump pulse to simulate the spontaneous Raman emission. The Raman fiber is a piece of 60 m long fiber according to the experiment. The GVD, $\beta_2$, and the nonlinear coefficient, $\gamma$, of the Raman fiber are set to 0.024 $ps^2/m$ and 0.005/W/m, respectively.

The simulation is a theoretical calculation of the laser pulse evolution along the Raman fiber, in which the Raman pulse is generated and amplified. In the simulation, the temporal window is 450 ps, and the corresponding spectral window is about 1500 nm, which ranges from 700 nm to 2200 nm. Most of the simulated results are obtained from a single simulation apart from the spectra.

## 4. SIMULATION RESULTS AND DISCUSSION

In the experiment, we have characterized the relation between the pump pulse and the first Raman Stokes pulse. So in the simulation, we investigate the pulse energy, spectrum, and temporal properties of the ASRE pulses with respect to the pump pulses.

Figure 4(a) plots the calculated output pulse energy versus pump pulse energy. As seen in Fig. 4(a), after the threshold, the Raman output increases almost linearly with respect to the pump. And it reaches a maximum at the threshold of the second Raman Stokes. These observations match the experiment well. There are discrepancies in the exact output energy and the threshold values, which we believe is due to the uncertainty in pump pulses and nonlinear coefficient of the Raman fiber. The uninformed exact temporal shape and chirp of the pulse in the experiment influence the Raman conversion greatly. The nonlinear coefficient depends on the exact mode field diameter of the fiber, which also varies from batch to batch.

The spectral evolution is also calculated in the simulation. Figure 4(b) shows the simulated evolution of the Raman light spectrum as the pump pulse energy increases. Compared with the experimental results in Fig. 2(b), the intensity of the pump pulse is higher in these spectra. The reason is that in the experiment there is a WDM filter after the Raman fiber to remove the residual pump, which is absent in the simulation. The evolution of the Raman light spectrum fits the experimental observation well qualitatively. The first Raman Stokes light increases quickly with increasing pump energy, and stops increasing after the second Raman Stokes is generated. However, the simulation results look noisier than the experimental results. That is because in the experimental measurement process the spectra are effectively averaged over several pulses.

The exact waveform of the picosecond pulses cannot be measured in the experiment. Autocorrelation measurement was used to characterize the time domain property of the pulses. Therefore, in the simulation, we calculate the autocorrelation traces of the output pulses for comparison with the experiments. A typical autocorrelation trace is shown in Fig. 5(a), which is similar to the experiment. The width and normalized height of the autocorrelation pedestal are plotted with respect to the pump pulse energy in Fig. 5(b). The width of the autocorrelation pedestal increases with the pump energy. At the highest pump, it decreases due to the generation of the second Raman Stokes. The normalized height of the autocorrelation pedestal increases with the pump. All these tendencies are the same as observed in the experiments. These simulation results reproduce the partially coherent noise-like pulse generation in ASRE well. It proves that the amplified spontaneous Raman emission process generates partially coherent noise-like pulses.

A pivotal advantage of numerical simulation is that it can reveal information that is not possible or easy to observe in the experiments. The pulse evolution along the optical fiber and the details of the pulse waveforms are examples.

Temporal and spectral evolutions of the pump and Raman pulse along the fiber are simulated, and the results for the case of 38 nJ pump energy are shown in Fig. 6. The ASRE starts from noise and becomes significant at a fiber length of about 15 m. The Raman pulse walks ahead of the pump pulse due to the normal chromatic dispersion at this wavelength band. The Raman pulse is not well defined due to the continuing conversion from the pump pulse along the fiber. Only the preceding

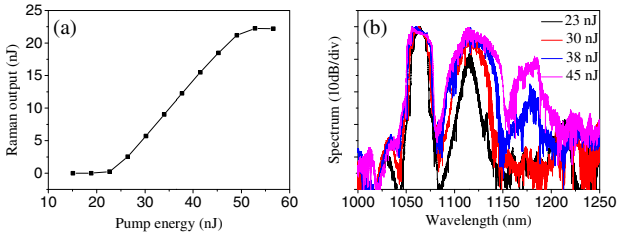


**Fig. 4.** (a) Pulse energy of the Raman light as a function of the pump pulse energy; (b) spectra of the Raman light at different pump pulse energies.

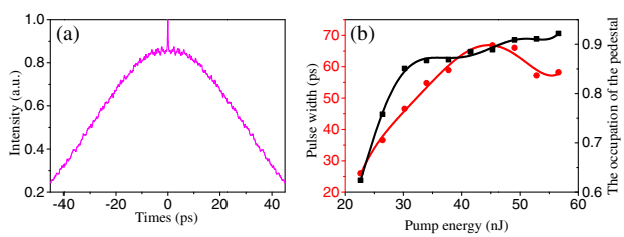


**Fig. 5.** (a) Autocorrelation function under the pump pulse energy of 30 nJ; (b) autocorrelation pedestal's pulse width (circle) and the normalized height (box) versus pump.

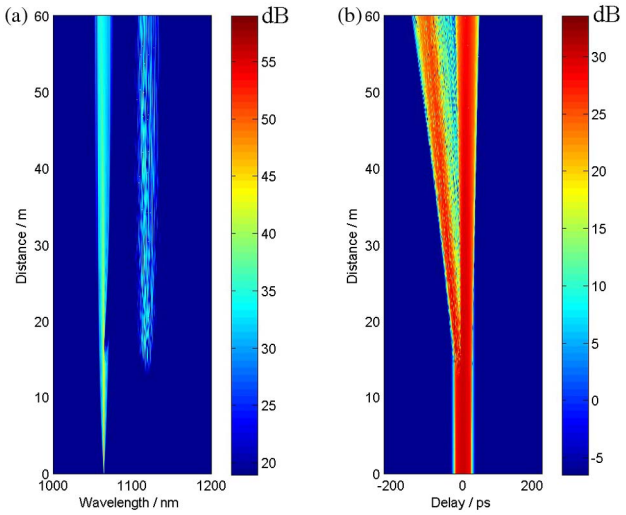


**Fig. 6.** (a) Spectral and (b) temporal evolutions of the laser pulse along the fiber.

part of the pump pulse is converted to Raman pulse while the tail of the pump pulse has no contribution to the Raman conversion, because of the dispersion-induced walk-off effect. The spectrum of the 1120 nm Raman pulse is broadband and tanglesome. The fluctuating nature of the output spectrum is related to the noise-like pulse output.

Figure 7(a) plots the calculated waveform of the laser pulse emitting at the end of the 60 m Raman fiber. Figure 7(b) is the waveform after filtering the pump light spectrally. The preceding part of the 1064 nm pump pulse is transferred to the Raman pulse and depleted significantly. The Raman pulse is indeed noise-like, which contains stochastic subpulses. And the Raman pulse exceeds the pump pulse for about 100 ps due to the normal chromatic dispersion.

In practice, the information on the evolution of the Raman pulse energy along the fiber is important for fiber length optimization, which is therefore investigated numerically as well. As shown in Fig. 8, with the increase of the fiber length, the Raman Stokes pulse grows quickly at a point where it reaches threshold, and saturates only after a few meters of propagation. The Raman Stokes pulse energy tends to be stable after 25 m, because of the walk-off effect. The Raman pulse and pump pulse become spatially separate at longer fiber length. Therefore, the fiber length of 60 m in the experiment is too long. A maximum of about 25 m is needed for efficient Raman conversion. Figure 8(a) plots the case of 38 nJ pump

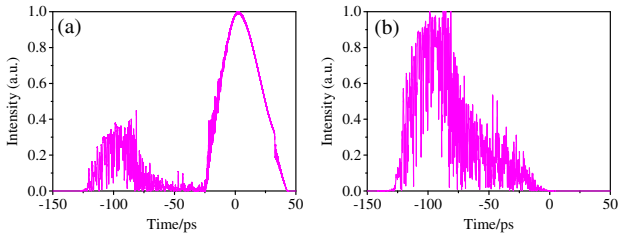


**Fig. 7.** Calculated waveform of (a) the laser pulse and (b) the Raman pulse (which are normalized to their peak values, respectively).

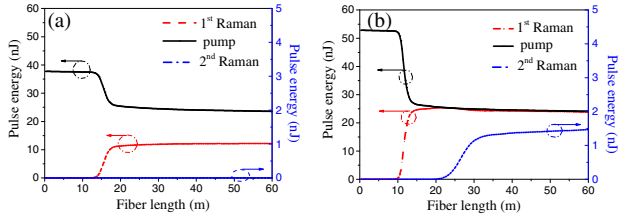


**Fig. 8.** Evolution of the Raman and pump pulse energy in the fiber at (a) 38 nJ pump pulse and (b) 53 nJ pump pulse, respectively. At 38 nJ pumping, the second Raman Stokes is negligible.

pulse, while Fig. 8(b) plots the case of 53 nJ pumping. The second Raman Stokes light is generated at higher pump energy, and it saturates quickly as well.

## 5. CONCLUSION

Amplified spontaneous Raman emission under short pulse pumping is a simple and economic way to generate a wavelength-agile ultrafast laser for various applications. The output pulse characteristics of amplified spontaneous Raman emission under picosecond pumping are investigated both experimentally and numerically. It is found that the Raman output pulses are noise-like with partial coherence, which has important implications for applications concerned with peak power and coherence. A model based on the generalized nonlinear Schrödinger equation is used to numerically simulate the process, which reproduces the finding and other experimental observations well. It proves that the amplified spontaneous Raman emission process generates partially coherent noise-like pulses. The numerical simulation also gives us insight on the Raman and pump pulse evolution along the fiber, which is helpful in designing the source.

**Funding.** National Natural Science Foundation of China (NSFC) (61575210).

## REFERENCES

1. G. J. Exarhos, M. Sun, V. E. Gruzdev, U. Eppelt, S. Russ, J. A. Menapace, D. Ristau, C. Hartmann, C. Siebert, M. J. Soileau, J. Zhu, and W. Schulz, "Laser ablation mechanism of transparent dielectrics with picosecond laser pulses," Proc. SPIE **8530**, 853007 (2012).
2. C. L. Hoy, O. Ferhanoglu, M. Yildirim, K. Ki Hyun, S. S. Karajanagi, K. M. C. Chan, J. B. Kobler, S. M. Zeitels, and A. Ben-Yakar, "Clinical ultrafast laser surgery: recent advances and future directions," IEEE J. Sel. Top. Quantum Electron. **20**, 242–255 (2014).
3. J. Serbin, T. Bauer, C. Fallnich, A. Kasenbacher, and W. H. Arnold, "Femtosecond lasers as novel tool in dental surgery," Appl. Surf. Sci. **197**, 737–740 (2002).
4. A. H. Zewail, "Femtochemistry atomic-scale dynamics of the chemical bond using ultrafast lasers," Angew. Chem. Int. Ed. **39**, 2586–2631 (2000).
5. J. Limpert, S. Hädrich, J. Rothhardt, M. Krebs, T. Eidam, T. Schreiber, and A. Tünnermann, "Ultrafast fiber lasers for strong-field physics experiments," Laser Photon. Rev. **5**, 634–646 (2011).
6. V. V. Yakovlev, G. I. Petrov, H. F. Zhang, G. D. Noojin, M. L. Denton, R. J. Thomas, and M. O. Scully, "Stimulated Raman scattering: old physics, new applications," J. Mod. Opt. **56**, 1970–1973 (2009).
7. P. T. Rakich, Y. Fink, and M. Soljačić, "Efficient mid-IR spectral generation via spontaneous fifth-order cascaded-Raman amplification in silica fibers," Opt. Lett. **33**, 1690–1692 (2008).

8. E. Landahl, D. Baiocchi, and J. R. Thompson, "A simple analytic model for noise shaping by an optical fiber Raman generator," Opt. Commun. **150**, 339–347 (1998).
9. A. Betlej, P. Schmitt, P. Sidereas, R. Tracy, C. G. Goedde, and J. R. Thompson, "Increased Stokes pulse energy variation from amplified classical noise in a fiber Raman generator," Opt. Express **13**, 2948–2960 (2005).
10. M. Horowitz, Y. Barad, and Y. Silberberg, "Noise like pulses with a broadband spectrum generated from an erbium-doped fiber laser," Opt. Lett. **22**, 799–801 (1997).
11. L. M. Zhao, D. Y. Tang, and J. Wu, "Noise-like pulse in a gain-guided soliton fiber laser," J. Opt. Soc. Am. **15**, 2145–2150 (2007).
12. S. Kobtsev, S. Kukarin, S. Smirnov, S. Turisyn, and A. Latkin, "Generation of double-scale femtopico-second optical lumps in mode-locked fiber lasers," J. Opt. Soc. Am. **17**, 20707–20713 (2009).
13. S. M. Kobtsev and S. V. Smirnov, "Fiber lasers mode-locked due to nonlinear polarization evolution: golden mean of cavity length," Laser Phys. **21**, 272–276 (2011).
14. S. V. Smirnov, S. M. Kobtsev, S. V. Kukarin, and S. K. Turitsy, *Mode-Locked Fibre Lasers with High-Energy Pulses* (Academic, 2011).
15. S. V. Smirnov, S. M. Kobtsev, and S. V. Kukarin, "Efficiency of nonlinear frequency conversion of double-scale pico-femtosecond pulses of passively mode-locked fiber laser," Opt. Express **22**, 1058–1064 (2014).
16. S. Kobtsev, S. Kukarin, S. Smirnov, and I. Ankudinov, "Cascaded SRS of single- and double-scale fiber laser pulses in long extra-cavity fiber," Opt. Express **22**, 20770–20775 (2014).
17. S. M. Kobtsev, S. V. Kukarin, and S. V. Smirnov, "Supercontinuum from single- and double-scale fiber laser pulses in long extra-cavity P2O5-doped silica fiber," Proc. SPIE **9347**, 93471 (2015).
18. S. M. Kobtsev, S. V. Kukarin, and S. V. Smirnov, "All-fiber high-energy supercontinuum pulse generator," Laser Phys. **20**, 375–378 (2010).
19. J. C. Hernandez-Garcia, O. Pottiez, and J. M. Estudillo-Ayala, "Supercontinuum generation in a standard fiber pumped by noise-like pulses from a figure-eight fiber laser," Laser Phys. **22**, 221–226 (2012).
20. A. Zaytsev, C. H. Lin, Y. J. You, C. C. Chung, C. L. Wang, and C. L. Pan, "Supercontinuum generation by noise-like pulses transmitted through normally dispersive standard single-mode fibers," Opt. Express **21**, 16056–16062 (2013).
21. S. S. Lin, S. K. Hwang, and J. M. Liu, "Supercontinuum generation in highly nonlinear fibers using amplified noise-like optical pulses," Opt. Express **22**, 4152–4160 (2014).
22. K. Tankala, S. Kobtsev, S. Kukarin, S. Smirnov, and Y. Fedotov, "Ultra-wide-tunable fibre source of femto- and picosecond pulses based on intracavity Raman conversion," Proc. SPIE **7580**, 758023 (2010).
23. S. V. Smirnov, J. D. Ania-Castanon, T. J. Ellingham, S. M. Kobtsev, S. Kukarin, and S. K. Turitsyn, "Optical spectral broadening and supercontinuum generation in telecom applications," Opt. Fiber Technol. **12**, 122–147 (2006).
24. S. Smirnov and S. Kobtsev, "Modelling of noise-like pulses generated in fibre lasers," Proc. SPIE **9732**, 97320S (2016).
25. M. Rhodes, G. Steinmeyer, J. Ratner, and R. Trebino, "Pulse-shape instabilities and their measurement," Laser Photon. Rev. **7**, 557–565 (2013).
26. J. M. Dudley and J. R. Taylor, *Supercontinuum Generation in Optical Fibers* (Academic, 2010).
27. K. J. Blow and D. Wood, "Theoretical description of transient stimulated raman scattering in optical fibres," IEEE J. Quantum Electron. **25**, 2665–2673 (1989).
28. R. H. Stolen, J. P. Gordon, W. J. Tomlinson, and H. A. Haus, "Raman response function of silica-core fibers," J. Opt. Soc. Am. B **6**, 1159–1166 (1989).
29. P. V. Mamyshev and S. V. Chernikov, "Ultrashort-pulse propagation in optical fibers," Opt. Lett. **15**, 1076–1078 (1990).
30. D. Hollenbeck and C. Cantrell, "Multiple-vibrational-mode model for fiber-optic Raman gain spectrum and response function," J. Opt. Soc. Am. B **19**, 2886–2892 (2002).
31. J. Hult, "A fourth-order Runge-Kutta in the interaction picture method for simulating supercontinuum generation in optical fibers," J. Lightwave Technol. **25**, 3770–3775 (2007).
32. D. Churin, J. Olson, R. A. Norwood, N. Peyghambarian, and K. Kieu, "High-power synchronously pumped femtosecond Raman fiber laser," Opt. Lett. **40**, 2529–2532 (2015).